Comparison of NLDAS-2 Simulated and NASMD Observed Daily Soil Moisture. Part II: Impact of Soil Texture Classification and Vegetation Type Mismatches

YOULONG XIA

National Centers for Environmental Prediction/Environmental Modeling Center, and I. M. System Group at NCEP/EMC, College Park, Maryland

MICHAEL B. EK

National Centers for Environmental Prediction/Environmental Modeling Center, College Park, Maryland

YIHUA WU

National Centers for Environmental Prediction/Environmental Modeling Center, and I. M. System Group at NCEP/EMC, College Park, Maryland

TRENT FORD AND STEVEN M. QUIRING

Department of Geography, Texas A&M University, College Station, Texas

(Manuscript received 9 May 2014, in final form 13 May 2015)

ABSTRACT

In this second part of a two-part paper, the impacts of soil texture and vegetation type misclassification and their combined effect on soil moisture, evapotranspiration, and total runoff simulation are investigated using the Noah model. The results show that these impacts are significant for most regions and soil layers, although they vary depending on soil texture classification, vegetation type, and season. The use of site-observed soil texture classification and vegetation type in the model does not necessarily improve anomaly correlations and reduce mean absolute error for soil moisture simulations. Instead, results are mixed when examining all regions and soil layers. This is attributed to the compensation effects (e.g., effect of ill-calibrated model parameters), as Noah has been more or less calibrated with model-specified soil texture classification and vegetation type. The site-based analysis shows that Noah can reasonably simulate the variation of daily evapotranspiration, soil moisture, and total runoff when soil texture classification (vegetation type) is corrected from loam (forest) to clay (grasslands) or vice versa. This suggests that the performance of Noah can be further improved by tuning model parameters when site-observed soil texture and vegetation type are used.

1. Introduction

It is well known that soil moisture variations in time and space are controlled by many factors such as soil texture, vegetation, and topography. In turn, soil moisture also affects the partitioning of net radiation into sensible heat and latent heat and the partitioning of precipitation into evapotranspiration (ET), surface runoff, and subsurface infiltration. Evaluating phase 2 of the North American Land Data Assimilation System (NLDAS-2) soil moisture using in situ observations is necessary for continued model improvement. Knowledge of the impact of misclassification of soil texture classification and vegetation type is important for understanding the spatial and temporal variations in NLDAS-2 performance. In the Noah land surface model, soil moisture is redistributed through infiltration, vegetation transpiration, and bare soil evaporation. Infiltration is the process of water, from sources such as rainfall and snowmelt, entering the soil. Vegetation transpiration is the process of water movement from plant uptake in the root zone through the leaves, stems, and flowers into the atmosphere. Evaporation is the process by which soil water changes state and moves from

Corresponding author address: Youlong Xia, IMSG at NCEP/EMC, NOAA Center for Weather and Climate Prediction, 5830 University Research Court, College Park, MD 20740.
E-mail: youlong.xia@noaa.gov

DOI: 10.1175/JHM-D-14-0097.1

the surface to the atmosphere. Soil moisture increases when inputs, including rainfall and snowmelt, exceed outputs, such as surface runoff, base flow, and evapotranspiration. Soil moisture decreases when outputs exceed inputs. Soil water storage and redistribution are a function of soil pore space and pore-size distribution, which are governed by soil texture. In general, fine-textured soils (i.e., those with high clay content) have higher porosity and total water holding capacity than coarse-textured soils (i.e., those with a high sand content).

Soil texture directly affects soil hydraulic conductivity, field capacity, and wilting point, which are important soil hydraulic parameters for soil moisture simulation. The water between field capacity and wilting point (i.e., plant-available water) can be used for plant uptake and evapotranspiration. Plant-available water is generally lower in coarse-textured soils (e.g., sands and loamy sands), as the large soil pores have limited ability to retain water, and higher for medium-textured soils (e.g., loams, sandy loams, silt loams, silts, clay loams, sandy clay loams, and silty clay loams) because they have an ideal combination of meso- and micropores. Hydraulic conductivity controls how fast water infiltrates into soil and how fast the water becomes base flow as a result of gravity drainage. For example, fine-textured soils tend to have a lower hydraulic conductivity than coarse-textured soils because coarse-textured soils have larger pores and lower tortuosity, both of which facilitate more rapid water movement. Soil texture determines total water storage, available water holding capacity, and water movement in soil. Therefore, soil texture directly affects soil moisture (both its magnitude and variability) and indirectly affects evapotranspiration and total runoff Q (Fernandez-Illescas et al. 2001; Wang et al. 2009).

Soil moisture is modified by evapotranspiration while evapotranspiration is controlled by rainfall interception, net radiation, advection, turbulent transport, leaf area, plant-available water capacity, and land surface parameters (McNaughton and Jarvis 1983; Santanello et al. 2013; Zhang et al. 2001). The relative importance of these factors depends on climate, soil, and vegetation conditions. Generally speaking, the principal controls on evapotranspiration are plant-available water and canopy resistance under dry conditions. In contrast, under wet conditions the dominant controls are advection, net radiation, leaf area, and turbulent transport. Under intermediate conditions, the relative importance of these factors varies depending on climate, soil, and vegetation (Zhang et al. 2001). Because water that is transpired comes from the soil, plants with deeper roots tend to have more constant transpiration rates because they can access a larger soil volume. Herbaceous plants (e.g., crops and grasses) generally transpire less than woody plants (e.g., trees and shrubs) because they usually have less extensive foliage (Swank and Douglass 1974) and more shallow roots. Tennant (1976) showed that the plant-available water in a wheat field depended more on rooting depth than on the soil hydraulic properties of the five different soils. Forests tend to produce more evapotranspiration than pasture and crops because they have deeper roots and a greater leaf area (Turner 1991; Nepstad et al. 1994; Hodnett et al. 1995). Vegetation mismatches can set the wrong rooting depth and leaf area index in land surface models, which will result in incorrect evapotranspiration simulation. In Noah, the root zone is set as the top 1-m soil layer for cropland, grassland, open shrubland, closed shrubland, and wooded grassland land-use classes. It is set as the top 2-m soil layer for mixed cover, deciduous broadleaf forest, deciduous needleleaf forest, evergreen broadleaf forest, and evergreen needleleaf forest.

Soil moisture influences both hydrology (e.g., surface runoff, base flow, and evapotranspiration) and soil thermodynamics (e.g., soil temperature, land surface temperature, and ground heat flux) in Noah. Seasonal variation of plant root density is highly dependent on mean root-zone soil temperature, as suggested by Dickinson et al. (1993), and variations in plant root density will cause seasonal variations in transpiration (Wei et al. 2013). This mechanism has been implemented in the NLDAS-2 Noah model (Chen et al. 1996; Ek et al. 2003) to make evaporation simulation more realistic (Wei et al. 2013). In addition, soil temperature and ground heat flux impact land surface temperature, which will further affect evapotranspiration (Ek and Holtslag 2004). Soil moisture influences soil thermodynamics, and this can indirectly affect evapotranspiration. It is clear that soil moisture is a key variable in the Noah water cycle, but it is also influential in the Noah energy cycle. Soil texture and vegetation type strongly affect soil moisture, evapotranspiration, and total runoff simulations through many complex linear and nonlinear physical processes (Figs. 1, 2). Therefore, it is important to investigate the impacts of soil texture and vegetation mismatches on soil moisture, evapotranspiration, and total runoff simulations. This study is the second part of our two-part paper. In the first part, in situ soil moisture measurements collected from the North American Soil Moisture Database (NASMD) are used to evaluate NLDAS-2 soil moisture products generated from the four land surface models (Xia et al. 2015). The next section describes the soil, vegetation, and validation data. A model description including Noah hydrology and thermodynamics is described in section 3, the results are presented in section 4, and conclusions are discussed in section 5.

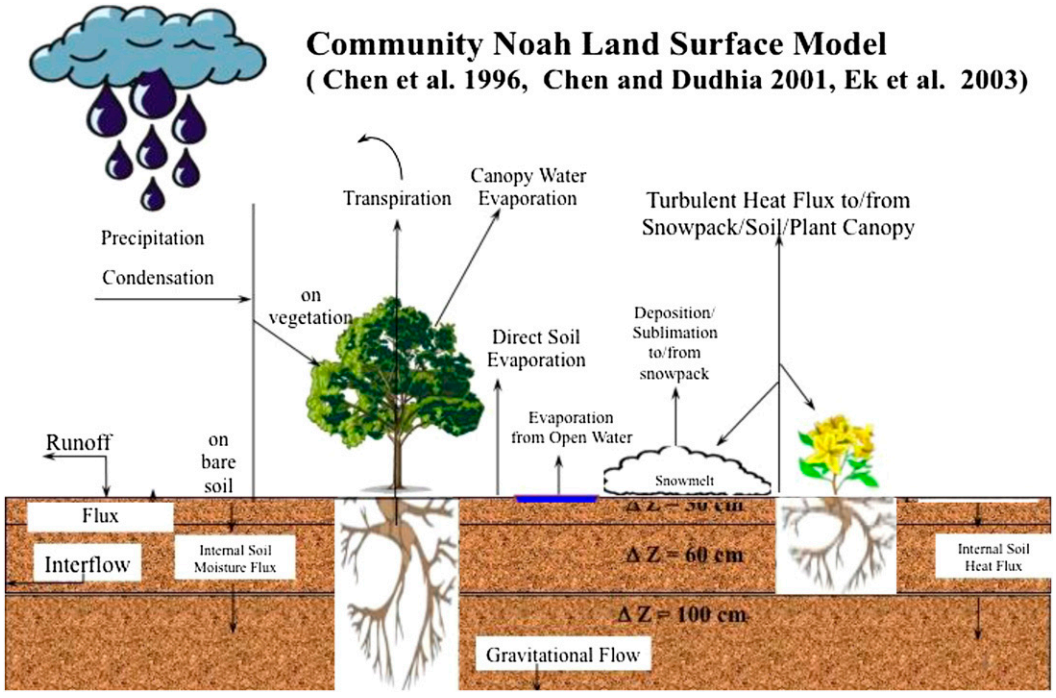

FIG. 1. Schematic diagram of Noah [modified from Chen and Dudhia (2001)].

2. Dataset descriptions

The soil texture database over the continental United States was derived from the 1-km State Soil Geographic (STATSGO) database of Miller and White (1998), which has 13 soil texture classes. The 13-category vegetation classification was derived from the global, 1-km, Advanced Very High Resolution Radiometer (AVHRR)-based database provided by the University of Maryland (UMD; Hansen et al. 2000). Daily soil moisture provided by NASMD in seven regions—Alabama (AL), Colorado (CO), Michigan (MI), Nebraska (NE), Oklahoma (OK), West Texas (WTX), and Utah (UT)—were used for validation. These data include 385 sites from seven soil moisture measurement networks (Nebraska Automated Weather Data Network, NOAA Climate Reference Network, Michigan Automated Weather Network, Oklahoma Mesonet, Snowpack Telemetry Network, Soil Climate Analysis Network, and West Texas Mesonet). More details about the networks and measurement accuracy can be found in Xia et al. (2015). Soil moisture data are available for 5–14 years, depending on the network.

3. Model and experiment design

a. *Noah hydrology*

In Noah, version 2.8, the prognostic equation for the volumetric soil moisture content Θ is

$$\frac{\partial \Theta}{\partial t} = \frac{\partial}{\partial z}\left(D\frac{\partial \Theta}{\partial z}\right) + \frac{\partial K}{\partial z} + F_{\Theta}, \quad (1)$$

where D is the soil water diffusivity given by $D = (bK_s\psi_s/\Theta_s)(\Theta/\Theta_s)^{b+2}$ (Ek 2005), K is hydraulic conductivity given by $K = K_s(\Theta/\Theta_s)^{2b+3}$ (Cosby et al. 1984), and F_{Θ} is source and sink (i.e., precipitation and evapotranspiration) for soil water. Variables K_s, ψ_s, Θ_s, and b are saturation hydraulic conductivity, air entry potential, soil porosity, and b parameter, respectively. They are determined by soil texture classes. A more accurate saturated hydraulic conductivity value was

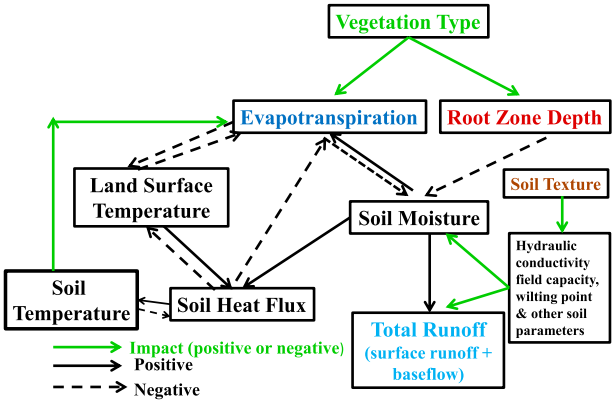

FIG. 2. Schematic diagram of the impact of soil texture and vegetation type on soil moisture, evapotranspiration, and total runoff.

computed during phase 2 of the Distributed Model Intercomparison Project (Smith et al. 2012), and that new value has since been implemented in Noah, version 2.8. The soil hydrology and thermodynamics described below are based on Noah, version 2.8. For brevity, we will refer to the model simply as Noah in the rest of the paper.

Noah includes four soil layers: 0–10, 10–40, 40–100, and 100–200 cm. For crop, grass, and shrublands, Noah sets the top three soil layers as the root zone. Equation (1) is integrated over the four soil layers and F_Θ is expanded to obtain

$$d_{z_1}\frac{\partial\Theta_1}{\partial t} = -D\left(\frac{\partial\Theta}{\partial z}\right)_{z_1} - K_{z_1} + P_d - Q_{\text{surf}} - E_{\text{dir}} - a_1E_t, \tag{2a}$$

$$d_{z_2}\frac{\partial\Theta_2}{\partial z} = D\left(\frac{\partial\Theta}{\partial z}\right)_{z_1} - D\left(\frac{\partial\Theta}{\partial z}\right)_{z_2} + K_{z_1} - K_{z_2} - a_2E_t, \tag{2b}$$

$$d_{z_3}\frac{\partial\Theta_3}{\partial z} = D\left(\frac{\partial\Theta}{\partial z}\right)_{z_2} - D\left(\frac{\partial\Theta}{\partial z}\right)_{z_3} + K_{z_2} - K_{z_3} - a_3E_t, \tag{2c}$$

and

$$d_{z_4}\frac{\partial\Theta_4}{\partial z} = D\left(\frac{\partial\Theta}{\partial z}\right)_{z_3} + K_{z_3} - K_{z_4}, \tag{2d}$$

where a_i is the ith soil layer weight coefficients $a_1 = d_{z_1}/(d_{z_1} + d_{z_2} + d_{z_3})$, $a_2 = d_{z_2}/(d_{z_1} + d_{z_2} + d_{z_3})$, and $a_3 = d_{z_3}/(d_{z_1} + d_{z_2} + d_{z_3})$; d_{z_i} is the ith soil layer thickness; P_d is the precipitation not intercepted by the canopy; Q_{surf} is the surface runoff; E_{dir} is the direct evaporation from bare soil; E_t is the canopy evapotranspiration; and K_{z_4} is the moisture loss due to gravitational percolation out of the fourth soil layer (i.e., base flow).

For forest types, Noah defines all four soil layers as the root zone. Therefore, the integrated Eq. (1) is written as

$$d_{z_1}\frac{\partial\Theta_1}{\partial t} = -D\left(\frac{\partial\Theta}{\partial z}\right)_{z_1} - K_{z_1} + P_d - Q_{\text{surf}} - E_{\text{dir}} - a_1E_t, \tag{3a}$$

$$d_{z_2}\frac{\partial\Theta_2}{\partial z} = D\left(\frac{\partial\Theta}{\partial z}\right)_{z_1} - D\left(\frac{\partial\Theta}{\partial z}\right)_{z_2} + K_{z_1} - K_{z_2} - a_2E_t, \tag{3b}$$

$$d_{z_3}\frac{\partial\Theta_3}{\partial z} = D\left(\frac{\partial\Theta}{\partial z}\right)_{z_2} - D\left(\frac{\partial\Theta}{\partial z}\right)_{z_3} + K_{z_2} - K_{z_3} - a_3E_t, \tag{3c}$$

and

$$d_{z_4}\frac{\partial\Theta_4}{\partial z} = D\left(\frac{\partial\Theta}{\partial z}\right)_{z_3} + K_{z_3} - K_{z_4} - a_4E_t, \tag{3d}$$

where $a_1 = d_{z_1}/(d_{z_1} + d_{z_2} + d_{z_3} + d_{z_4})$, $a_2 = d_{z_2}/(d_{z_1} + d_{z_2} + d_{z_3} + d_{z_4})$, $a_3 = d_{z_3}/(d_{z_1} + d_{z_2} + d_{z_3} + d_{z_4})$, and $a_4 = d_{z_4}/(d_{z_1} + d_{z_2} + d_{z_3} + d_{z_4})$.

In Eqs. (2) and (3), the direct evaporation from the bare soil is represented as

$$E_{\text{dir}} = (1 - \upsilon)\min\left[-D\left(\frac{\partial\Theta}{\partial z}\right)_{z_1} - K_{z_1}, E_p\right], \tag{4}$$

and the canopy evapotranspiration is represented as

$$E_t = \upsilon E_p B_c\left[1 - \left(\frac{W_c}{S}\right)^n\right], \tag{5}$$

where E_p is the potential evaporation; υ is the green vegetation fraction; W_c is the intercepted canopy water content; S is the maximum allowed W_c value (interception capacity); $n = 0.5$; and B_c is the resistance term including canopy resistance, reflecting soil moisture stress.

The variable B_c is represented as (Ek and Mahrt 1991; Chen et al. 1996)

$$B_c = \frac{1 + (\Delta/R_r)}{1 + R_cC_h + (\Delta/R_r)}, \tag{6}$$

where C_h is the surface exchange coefficient for heat and soil moisture; R_r is a function of surface air temperature, surface pressure, and C_h; R_c is the canopy resistance including soil moisture stress function F_4 (defined below) with a range from 0 to 1; and Δ depends on the slope of the saturation specific humidity curve.

Noah uses a Jarvis-type model (Jarvis 1976) to calculate R_c. The formulation is expressed as a minimum resistance multiplied by a series of independent stress functions (Jacquemin and Noilhan 1990):

$$R_c = \frac{R_{c_{\min}}}{\text{LAI}F_1F_2F_3\delta F_4}, \tag{7}$$

$$F_1 = \frac{(R_{c_{\min}}/R_{c_{\max}}) + f}{1 + f} \quad \text{where} \quad f = 0.55\frac{R_g}{R_{g_l}}\frac{2}{\text{LAI}},$$

$$F_2 = \frac{1}{1 + [q^*(T_a) - q_a]},$$

$$F_3 = 1 - B1(T_{\text{ref}} - T_a)^2,$$

and

$$F_4 = \sum_{i=1}^{4} \frac{(\Theta_i - \Theta_w)d_{z_i}}{(\Theta_{\text{ref}} - \Theta_w)(d_{z_1} + d_{z_2} + d_{z_3} + d_{z_4})},$$

where $R_{c_{\min}}$ is the minimum canopy resistance, $R_{c_{\max}}$ is the maximum canopy resistance, and LAI is the leaf area index with seasonal variation for a given vegetation type. The seasonal factor δ represents the seasonal variation of root distribution for a given vegetation class. The functions F_1, F_2, F_3, and F_4 vary from 0 to 1 and represent the effects of solar radiation, vapor pressure deficit, air temperature, and soil moisture, respectively. Variable R_g is the incoming solar radiation, and R_{g_l} is a lower limit of 30 W m^{-2} for forests and 100 W m^{-2} for crops (Noilhan and Planton 1989). The $B1$ is an empirical coefficient (0.0016). Here $q^*(T_a)$ is the surface saturated specific humidity, q_a is the surface specific humidity, T_{ref} is the reference air temperature, T_a is the air temperature, and Θ_{ref} and Θ_w are the field capacity and wilting point of soil moisture for a given soil texture. The seasonal LAI is calculated depending on vegetation classes as

$$\text{LAI} = \text{LAI}_{\min} + \beta(\text{LAI}_{\max} - \text{LAI}_{\min}), \tag{8}$$

where $\beta = (\upsilon - \upsilon_{\min})/(\upsilon_{\max} - \upsilon_{\min})$; $\upsilon_{\max}$ and $\upsilon_{\min}$ are the annual maximum and minimum vegetation fraction at each grid point, respectively (Wei et al. 2013); and $\text{LAI}_{\max}$ and $\text{LAI}_{\min}$ are the maximum and minimum LAI, respectively [obtained from Koster and Suarez (1996)]. The seasonal factor is calculated following the formulation suggested by Dickinson et al. (1993):

$$\delta = 1 - 0.0016(T_{\text{opt}} - T_{g_m})^2, \tag{9}$$

where T_{opt} is the optimum root growth temperature (298 K) and T_{g_m} is the mean soil temperature over the root zone depending on vegetation classes.

In Eqs. (2a) and (3a), Q_{surf} is represented as (Schaake et al. 1996)

$$Q_{\text{surf}} = \frac{P_d^2}{(P_d + I_c)}, \tag{10}$$

where I_c is the maximum infiltration, calculated by

$$I_c = \Theta_b[1 - \exp(-K\Delta t)], \tag{11}$$

where Θ_b is the total column soil moisture and Δt is the time step.

b. Noah thermodynamics

The land surface temperature T_s is determined by a single linearized surface energy balance equation representing the combined ground–vegetation surface (Mahrt and Ek 1984). The surface energy balance can be expressed as

$$(1 - \alpha)S_\downarrow + L_\downarrow - \sigma T_s^4 = H + \text{LH} + G, \tag{12}$$

where $S_\downarrow$ is downward shortwave radiation, $L_\downarrow$ is downward longwave radiation, σT_s^4 is upward longwave radiation (1 is used in Noah for emissivity), and α is surface albedo (bare soil or vegetation). Variable H is sensible heat flux, LH is latent heat flux (i.e., energy used for evaporation from bare soil and canopy, transpiration, and sublimation on snow surface), and G is ground heat flux. Using $\sigma T_s^4 \approx \sigma T_a^4\{1 + 4[(T_s - T_a)/T_a]\}$ and $G = -\lambda_T[(T_s - T_{g_1})/\Delta z]$, we can solve for T_s in Eq. (12) as

$$T_s = \frac{\left(F + 3\sigma T_a^4 - H - \text{LH} - \dfrac{\lambda_T T_{g_1}}{\Delta z}\right)}{\left(4\sigma T_a^3 - \dfrac{\lambda_T}{\Delta z}\right)}, \tag{13}$$

where $F = (1 - \alpha)S_\downarrow + L_\downarrow$, T_a is 2-m air temperature, λ_T is the soil thermal conductivity, T_{g_1} is the soil temperature at the first soil layer, and Δz is the midpoint of the first soil layer. There is a negative feedback between T_s and LH, as shown in Eqs. (12) and (13).

Land surface temperature is controlled by sensible heat flux, latent heat flux, ground heat flux, net incoming shortwave radiation, and downward longwave radiation. Latent heat flux and ground heat flux are closely related to soil moisture content, which has been discussed in section 3a. Soil temperature is controlled by the ground heat flux through a diffusion equation:

$$C_\Theta \frac{\partial T_g}{\partial t} = \frac{\partial}{\partial z}\left(\lambda_T \frac{\partial T_g}{\partial z}\right), \tag{14}$$

where T_g is the soil temperature and C_Θ is the volumetric heat capacity of soil. Variable C_Θ is a linear function of soil moisture content and λ_T is a nonlinear function of soil moisture that increases by several orders of magnitude from dry to wet soil conditions. The layer-integrated form of Eq. (14) for the ith soil layer is

$$\Delta z_i C_{\Theta_i} \frac{\partial T_{g_i}}{\partial t} = \left(\lambda_T \frac{\partial T_g}{\partial z}\right)_{z_{i+1}} - \left(\lambda_T \frac{\partial T_g}{\partial z}\right)_{z_i}. \tag{15}$$

In the top soil layer, the last term in Eq. (15) represents the surface ground heat flux and is calculated using the land surface temperature. The gradient at the bottom of the model is computed from a user-specified constant boundary temperature (data were provided by the Noah group). Therefore, soil moisture affects soil temperature and ground heat flux. These feedbacks will further affect

the land surface temperature and evaporation and/or evapotranspiration.

Analysis of Eqs. (1)–(15) shows that the physical processes affecting soil moisture are complicated. In general, soil texture determines soil hydraulic conductivity, soil porosity (field capacity), and wilting point. These soil hydraulic parameters modulate soil moisture. Soil moisture change will affect evapotranspiration through F_4 in Eq. (7). Changes in evapotranspiration will inversely affect soil moisture through the right term in Eqs. (2) and (3) for the entire root zone. In addition, vegetation type can affect soil moisture by changing rooting depth. It also constrains evapotranspiration through canopy resistance and LAI, which further affects soil moisture. Soil temperature also influences evapotranspiration through seasonal variations of root distribution. Soil moisture affects soil temperature through λ_T and C_Θ, and it affects sensible heat flux (SH) and land surface temperature. Figure 2 details how soil texture and vegetation type affect soil moisture and the other state variables and fluxes.

c. Soil and vegetation parameters setup

In NLDAS-2, the soil texture over the continental United States was derived from the 1-km STATSGO database. Noah assumes a vertically uniform soil texture class based on the predominant soil texture of the top 5-cm layer. Outside of the continental United States, the soil texture database was derived from the 5-min Agricultural Research Service and Food and Agriculture Organization (ARS FAO) data of Reynolds et al. (2000). For each 1/8° grid cell in NLDAS-2, the most common FAO soil class is used. Several soil physical and hydrological parameters used in hydrology and thermodynamics are prescribed through the Noah lookup tables. These include soil porosity, reference soil water content (field capacity equivalent), permanent wilting point, saturated hydraulic conductivity, b parameter, saturated soil water diffusivity, and air entry soil matric potential, among others. These parameters are dependent on soil texture classes, and they are computed based on the work of Cosby et al. (1984), except for K_s, which is based on the work of Rawls et al. (1991). These parameters, similar to soil texture classes, are uniform for all four soil layers.

The vegetation classification was derived from the global 1-km UMD database. For each 1/8° grid cell, the most common vegetation type is used for each grid cell. The vegetation parameters related to Noah soil hydrology and thermodynamics, such as root depth, root density, minimum stomatal resistance, roughness length, green vegetation fraction, and leaf area index are obtained either from satellite retrievals or from the Noah lookup tables. More information about the soil and vegetation database, including maps and tables, may be viewed on the NLDAS website (http://www.emc.ncep.noaa.gov/mmb/nldas/LDAS8th/soils/LDASsoils.shtml and http://www.emc.ncep.noaa.gov/mmb/nldas/LDAS8th/MAPPED.VEG/LDASmapveg.shtml).

d. Experiment design and spinup

Noah output from NLDAS-2 was used as a benchmark (control run, hereafter called Crun) in this study (e.g., Xia et al. 2012a,b). In addition, three sensitivity tests were conducted. The first test uses site-specific soil texture from 385 NASMD sites to replace default soil texture in the control run (hereafter called Srun). The second test uses site-specific vegetation type to replace the default vegetation type in the control run (hereafter called Vrun), and the third test uses both the site-specific soil texture and vegetation type to replace the default types in the control run (hereafter called SVrun). It should be noted that only grid points with NASMD information were used in the three sensitivity experiments. To minimize the effect of initial conditions such as soil moisture, soil temperature, canopy water content, and snowpack on Noah simulations, we used the initial conditions from 1 January 1989 obtained from a Noah control run and ran each simulation to 1 January 1999 (10-yr spinup). We used the output from 1 January 1999 to 31 December 2012 to calculate statistics for the comparative analysis. NLDAS-related experiments have demonstrated that a 10-yr spinup is sufficient to overcome the impact of the initial conditions on Noah simulations (Cosgrove et al. 2003; Xia et al. 2012a).

The statistics used in this study are daily anomaly Pearson correlations AC, root-mean-square error RMSE, and mean absolute error MAE, as used in the previous studies from Xia et al. (2014, 2015). To investigate if the difference between the sensitivity tests and Noah control is significant at the 95% confidence level, we calculated the confidence interval (CI) for AC and RMSE. For daily AC, we first converted the AC value to z' using Fisher's z' transformation (Hotelling 1953) calculator (http://onlinestatbook.com/2/calculators/r_to_z.html), then computed a CI in terms of z', and finally converted the CI back to AC. To test if two dependent correlations are significantly different, we used the three correlation coefficients and their associated sample sizes to compute the probability value and the z score (Steiger's z test; Steiger 1980; Saville 1990). A probability value of less than 0.05 indicates that the two correlation coefficients are significantly different from each other. For the calculation of RMSE at the 95% confidence level, we first compute RMSE for a given period and then compute the standard deviation S_d for a time series

$$S_d = \sqrt{\frac{\sum_{i=1}^{i=N} (|\mathrm{SM}_i - O_i| - \mathrm{RMSE})^2}{N-1}}, \quad (16)$$

where SM and O are the simulated and observed daily soil moisture, respectively, and N is the number of days in the measured records. The RMSE CI (Congalton and Green 2009) at the 95% confidence level is expressed as

$$\mathrm{RMSE} \pm 1.96(\mathrm{SRMSE}), \quad (17)$$

where $\mathrm{SRMSE} = S_d/\sqrt{N}$. The CI varies from RMSE − 1.96(SRMSE) to RMSE + 1.96(SRMSE) at the 95% confidence level. We compute CIs for each experiment in addition to Crun. Statistical significance is then determined by whether both CIs overlap. If both CIs overlap, this suggests that the sensitivity test is not significant. Otherwise, it is significant at the 95% confidence level. This method has been previously used to assess the statistical significance of soil moisture assimilation on water fluxes (e.g., total runoff) and state variables (e.g., soil moisture and soil temperature) in Noah (Kumar et al. 2009, 2014). In addition, the signed change in MAE was computed for each day in the study period, and a two-sample Student's t test was used to assess whether the mean change in MAE was significantly different from zero (at the 95% confidence level).

4. Results

The soil texture parameter used in NLDAS-2 is compared with the corresponding texture information from the observations (NASMD; Fig. 3). The representativeness of NLDAS-2 soil texture varies by region, with generally good correspondence in CO, MI, and UT and somewhat weaker correspondence in NE, OK, and WTX. The largest differences in soil texture are in AL, where all but one site are classified as having sandy loam soils in NLDAS-2. The corresponding observed soil textures for these sites range from clay to loamy sand.

Differences in land cover between NLDAS-2 and NASMD (Fig. 4) are consistently larger than those in soil texture. Some of this is due to preferential siting of the observation sites. For example, NASMD-reported land cover in AL, OK, MI, and WTX are predominantly grassland, as the networks in these regions prefer to establish sites in locations with grassland vegetation (Schroeder et al. 2005; Illston et al. 2008). Grassland is generally representative of surrounding land cover in most of WTX, but it is less representative in the agricultural regions of OK and MI and the forested regions of AL and MI. This may explain the better correspondence of land cover types between NLDAS-2 and NASMD in WTX as compared with AL, OK, and MI. In CO and UT, the majority of NASMD-reported land cover is mixed forest cover, while the NLDAS-2 classified types are more frequently woodland, grassland, and evergreen needle leaf forest. Not surprisingly, NLDAS-2 land cover in NE is dominated by cropland and, to a lesser extent, grassland. However, NASMD-reported vegetation is more frequently closed shrubland. Another reason for lack of correspondence is because of the coarse resolution of the NLDAS-2 domain, as it could easily be nonrepresentative of the point location information.

a. *Impact of soil texture and vegetation type mismatch*

1) IMPACTS ON SOIL MOISTURE SIMULATION

(i) Soil moisture variability

Differences in daily soil moisture variations (correlations) between Crun and the sensitivity tests (Srun, Vrun, and SVrun) and the significance of these differences vary by region (Table 1). Updating only soil texture parameters in Noah (Srun) resulted in significantly higher soil moisture correlations (i.e., improvement) at the 25-cm depth in NE and the 5-cm depth in WTX, while showing no improvement in CO, OK, and UT. Not surprisingly, using observed soil texture resulted in significant increases in soil moisture correlations at all depths in AL, where differences between NLDAS-2 and NASMD soil textures were greatest. Srun resulted in a large decrease in correlations at the 5-cm depth in MI, suggesting that the default NLDAS-2 soil texture is more representative of actual conditions than the site-specific soil texture.

Updating only land cover parameters in Noah (Vrun) resulted in significant improvements in modeled soil moisture variability at the 5-cm depth in CO, the 25-cm depth in NE, and the 5-cm depth in WTX. Correlations at all depths in OK increased significantly in Vrun, corresponding with the lack of correspondence between NLDAS-2 and NASMD vegetation types. Correlations at the 5- and 25-cm depths in AL increased significantly in Vrun, but the 70-cm soil moisture correlations decreased significantly. This could be attributable to differences in root-zone depth and corresponding ET variations and is explored in more detail in section 4a(2).

Changing Noah soil texture and vegetation parameters separately produced mixed results. In some regions the accuracy of the modeled soil moisture increased, while other regions showed no change or even deterioration in model performance. Therefore, it is no surprise that the combined SVrun shows similar variability with respect to improvements in the accuracy of model-simulated soil

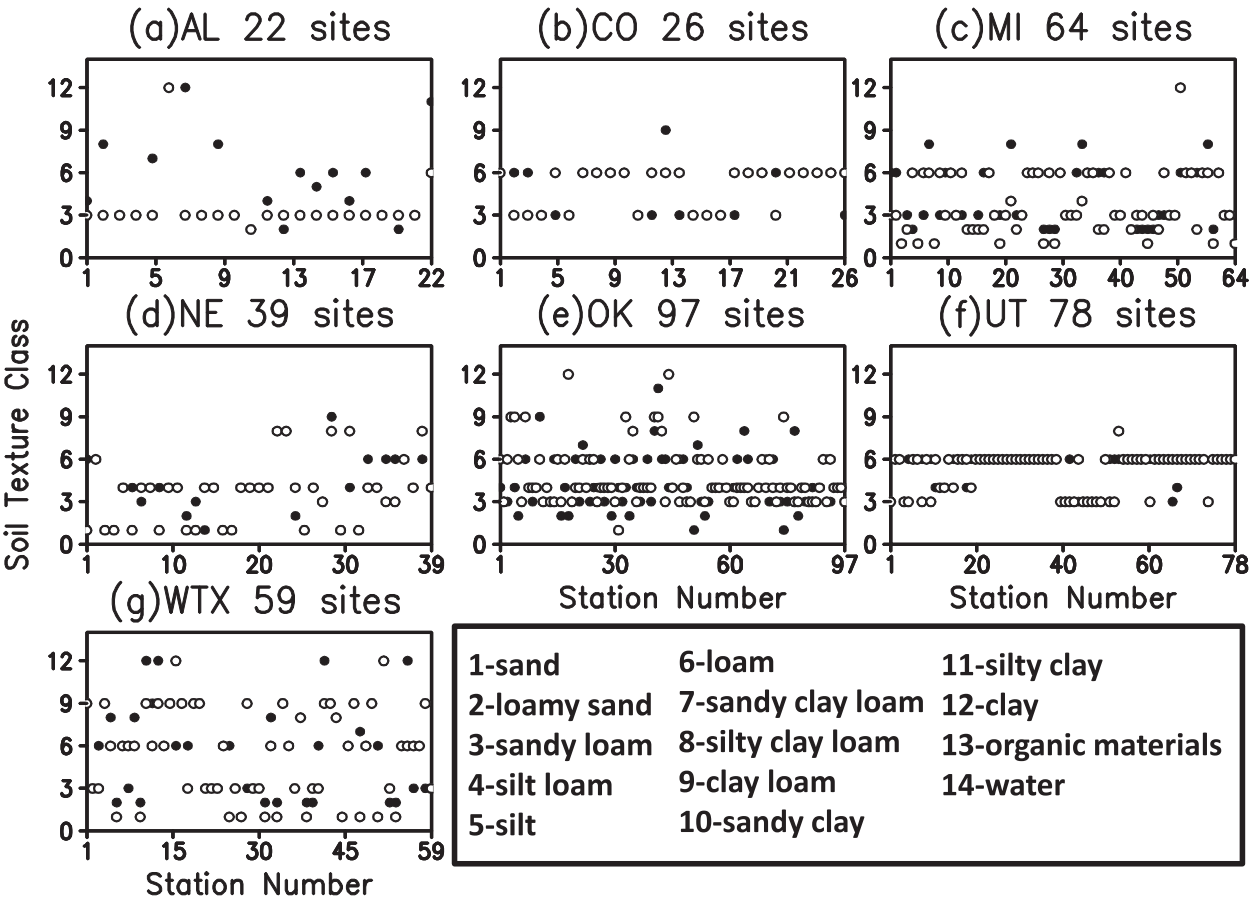

FIG. 3. Comparison of site-observed soil texture (solid circle) from NASMD and model-used soil texture from NLDAS-2 (open circle) for 385 sites in the seven regions.

moisture. SVrun resulted in significantly increased correlations at all depths in AL, mostly as a function of changes in soil texture. Significant improvements in SVrun were also seen at the 5-cm depth in CO, the 25-cm depth in NE, the 25- and 70-cm depths in OK, and the 5-cm depth in WTX. Significant decreases in correlations are seen in the 25-cm depth in CO, the 5-cm depth in MI (mostly as a function of changes in soil texture), and the 25-cm depth in WTX. Overall, Srun, Vrun, and SVrun resulted in more statistically significant improvements in model performance, but there was substantial spatial variability.

(ii) Soil moisture magnitude

The changes in the strength of the correlations between observed and model-simulated soil moisture anomalies are used to identify changes in model performance. In this section, we detail significant changes in MAE corresponding to Srun, Vrun, and SVrun (Table 2), which represent improvements or deteriorations in the magnitude of model-simulated soil moisture. The RMSE statistics were very similar to those of MAE, in spite of some differences, and are therefore listed Table 3. Updating only the soil texture parameter (Srun) resulted in significant improvements in MAE at the 25- and 70-cm depths in AL, the 25-cm depth in NE, and all depths in WTX. It should be noted that Srun model soil moisture improvements in WTX and NE are on average less than $0.005\,m^3\,m^{-3}$, whereas significant improvements in AL are much larger, with an average of $0.02\,m^3\,m^{-3}$. Small but statistically significant increases in MAE (deterioration) occurred at all depths in CO and OK for Srun.

Updating only the vegetation parameter (Vrun) resulted in significant improvements in MAE at the 5-cm depth in AL, CO, and UT; the 25-cm depth in NE; and both the 25- and 70-cm depths in WTX. Similar to Srun, significant deterioration is seen at all depths in OK. Interestingly, soil moisture at the 25- and 70-cm depths in AL had significant improvements (decreased MAE) in Srun, but it showed significant deterioration (increased MAE) in Vrun. Changing the soil texture in AL resulted in improved model performance, whereas changing the vegetation type resulted in decreased

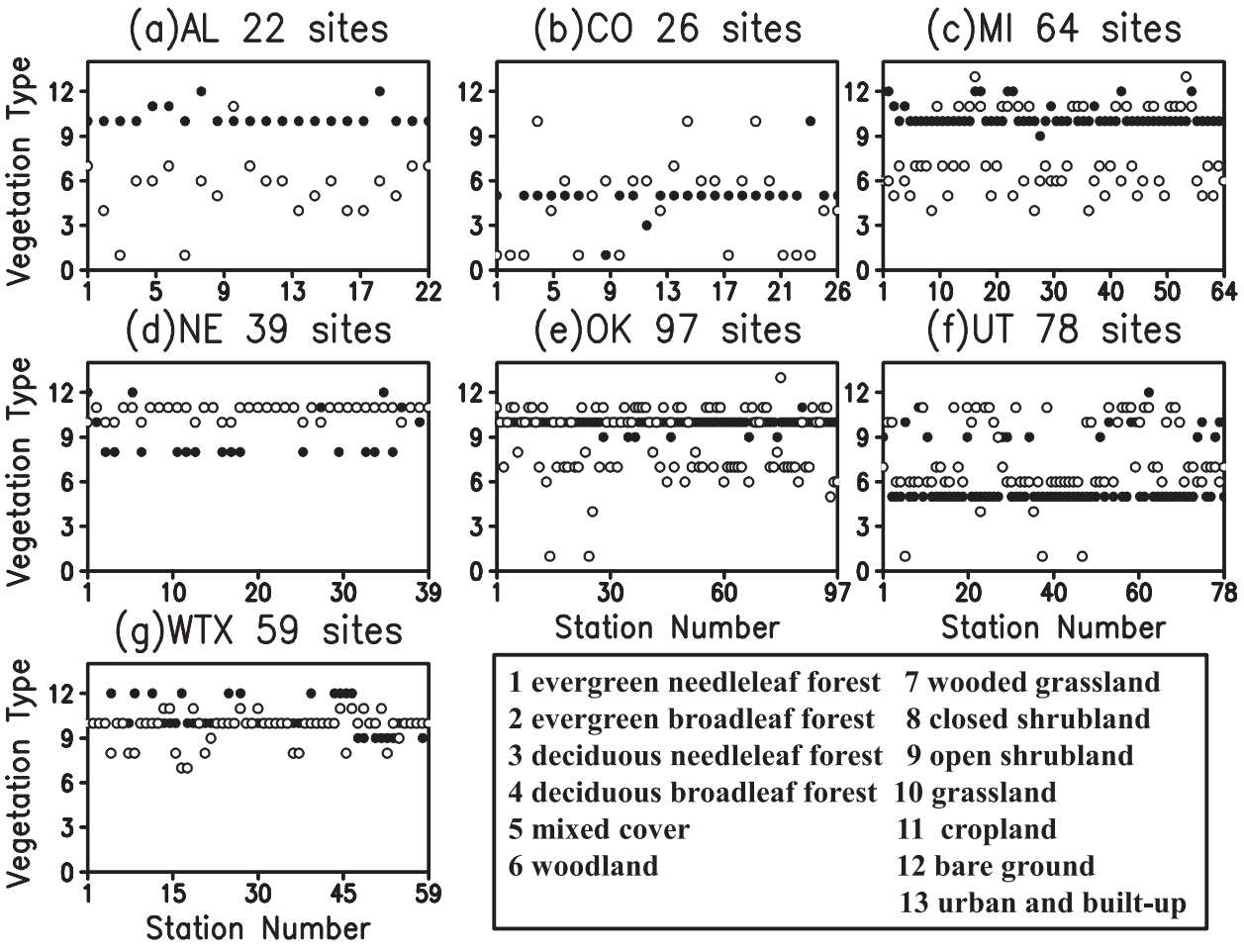

FIG. 4. Comparison of site-observed vegetation type (solid circle) from NASMD and model-used vegetation type from NLDAS-2 (open circle) for 385 sites in the seven regions.

performance. It is also interesting that changes in vegetation type (Vrun) resulted in increased correlations in OK, but also increased MAE. This suggests that prescribing the site-specific vegetation type in OK improves the model's ability to capture soil moisture variability and simultaneously increases model error.

The combined effect of soil texture and vegetation changes (SVrun) resulted in significant improvements in modeled soil moisture magnitude at the 5-cm depth in AL, CO, and UT; the 25-cm depth at NE; and the 25- and 70-cm depths at WTX. Improvements in soil moisture magnitude from Srun at the 25- and 70-cm depths in AL are offset by deteriorations from Vrun at the same depths, resulting in significant increases in MAE for SVrun. This also occurs at the 5-cm depth in WTX, although there are much smaller changes in MAE between Srun and Vrun. In general, changes in the soil texture and vegetation type have variable impacts on Noah's ability to accurately simulate soil moisture variability and magnitude. These variations are attributable to the original differences in soil texture and vegetation type between NLDAS-2 and NASMD. For example, changing the soil texture parameter in AL had a much more beneficial impact on soil moisture variability and magnitude than changing the vegetation type.

(iii) Seasonal variation

Our results show that soil texture and vegetation type mismatches have a significant impact on correlation and the MAE and RMSE values of the simulated daily soil moisture for all seven regions. The impact is specific to the soil layers and regions that were examined here. This section will discuss how these impacts vary on a monthly and seasonal basis. For a given month and soil depth, the soil moisture anomalies were combined together for all available years (i.e., 5–14 years) to compute the correlation. There were at least 140 (i.e., 28×5 in February with a 5-yr period) sample data pairs for this calculation. Therefore, the anomaly correlation is significant at the 95% confidence level when the value is larger than 0.20

TABLE 1. Correlations between simulated and observed daily soil moisture anomaly for Crun, Srun, Vrun, and SVrun in the seven regions. The values that have significant differences between tests and Noah control at the 95% confidence level are represented in boldface (improvement in italics).

Soil layer	Crun (lower limit, upper limit)	Srun	Vrun	SVrun
AL				
5 cm	0.42 (0.39, 0.44)	*0.56*	**0.46**	*0.58*
25 cm	0.57 (0.55, 0.59)	*0.70*	*0.63*	*0.72*
70 cm	0.51 (0.49, 0.53)	*0.62*	**0.47**	*0.56*
CO				
5 cm	0.55 (0.53, 0.58)	0.57	*0.67*	*0.70*
25 cm	0.67 (0.65, 0.69)	0.66	0.66	**0.63**
MI				
5 cm	0.67 (0.65, 0.69)	**0.59**	0.65	**0.58**
NE				
5 cm	0.25 (0.20, 0.29)	0.26	0.21	0.21
25 cm	0.66 (0.63, 0.69)	*0.83*	*0.86*	*0.86*
70 cm	0.88 (0.86, 0.89)	0.88	0.88	0.88
OK				
5 cm	0.80 (0.79, 0.81)	0.80	*0.82*	0.81
25 cm	0.85 (0.84, 0.86)	0.84	*0.87*	*0.87*
70 cm	0.89 (0.89, 0.90)	0.90	*0.91*	*0.91*
WTX				
5 cm	0.84 (0.83, 0.85)	*0.86*	*0.88*	*0.86*
25 cm	0.89 (0.88, 0.90)	0.90	**0.84**	**0.86**
70 cm	0.88 (0.87, 0.89)	0.88	**0.85**	0.89
UT				
5 cm	0.68 (0.66, 0.70)	0.69	0.69	0.68
25 cm	0.71 (0.69, 0.73)	0.71	0.70	0.70

TABLE 2. Values of MAE ($m^3 m^{-3}$) between simulated and observed daily soil moisture for Crun, Srun, Vrun, and SVrun in seven states. The value that has a significant difference between tests and Noah control at the 95% confidence level is represented in boldface (reduction in italics, two-sample Student's *t* test).

Soil layer	Crun	Srun	Vrun	SVrun
AL				
5 cm	0.0583	0.0582	*0.0556*	*0.0554*
25 cm	0.0604	*0.0418*	**0.0710**	*0.0505*
70 cm	0.1008	*0.0777*	**0.1370**	**0.1072**
CO				
5 cm	0.0446	**0.0454**	*0.0415*	*0.0417*
25 cm	0.0562	**0.0589**	**0.0632**	**0.0656**
MI				
5 cm	0.0315	0.0320	**0.0325**	0.0316
NE				
5 cm	0.0195	0.0204	**0.0227**	**0.0242**
25 cm	0.0129	0.0127	*0.0121*	0.0125
70 cm	0.0281	0.0281	0.0281	0.0281
OK				
5 cm	0.0320	**0.0404**	**0.0339**	**0.0423**
25 cm	0.0432	**0.0532**	**0.0490**	**0.0594**
70 cm	0.0553	**0.0674**	**0.0684**	**0.0840**
WTX				
5 cm	0.0265	*0.0257*	**0.0268**	**0.0277**
25 cm	0.0352	*0.0280*	*0.0318*	*0.0279*
70 cm	0.0306	*0.0245*	*0.0235*	*0.0194*
UT				
5 cm	0.0616	0.0614	**0.0629**	**0.0630**
25 cm	0.0540	0.0541	**0.0617**	**0.0619**

(Reichle et al. 2004; Xia et al. 2015). The variation in correlations for Crun and differences in correlations between the three sensitivity tests are shown in Fig. 5. If the difference is >0.05 or <-0.05, the impact of soil texture and vegetation type on the correlation is significant at the 95% confidence level. The results show significant differences in correlations between Srun, Vrun, and SVrun in all regions except for OK. Monthly variability in differences between runs are highest in AL and WTX, where large (small) positive differences occur from September to May (from June to August) in SVrun. Consistent with Tables 1 and 2, changes in soil texture have a larger impact on soil moisture correlations, particularly in AL, NE, and WTX.

Table 4 shows the seasonal variation of Crun daily correlations for different soil depths in CO, MI, and UT. Even though the correlations vary by region, month, and depth, all correlation coefficients are significant at the 95% confidence level. Corresponding differences of the correlations between sensitivity tests (Srun, Vrun, and SVrun) and Crun (Fig. 6) show either positive values or negative values outside ± 0.05, indicating that the changes are statistically significant. Mismatches in vegetation type have significant impacts in CO and UT, while soil texture mismatches have significant impacts in MI.

Variations in MAE by month and soil depth for Crun, and the MAE differences between the three tests (Srun, Vrun, and SVrun) and Crun, are also calculated for AL, NE, OK, and WTX (Fig. 7). In general, MAE values are smaller in the summer than in the winter, consistent with reduced volumetric water content in the summer season in these regions. Mismatches in soil texture significantly reduce MAE in AL and WTX and significantly increase MAE in OK. In contrast, mismatches in vegetation type significantly increase MAE in AL and OK, particularly during the warm season and in the deeper soil layers. The monthly variations in MAE can be seen for SVrun in all four regions, although the differences in MAE are not significant in NE (Fig. 7). The comparison between Srun and Vrun shows that the latter has a larger impact on soil moisture magnitude. Certainly combined effects (i.e., SVrun) mainly come from the effect of vegetation type change. Similar results are found in CO, MI, and UT (Fig. 8), although most of them do not have significant MAE differences.

Overall, mismatches in soil texture and vegetation type have significant effects on soil moisture variability and magnitude in most regions, but do not always lead to improvements. The mismatches in vegetation tend to have a larger impact on soil moisture magnitude,

TABLE 3. Values of RMSE ($m^3 m^{-3}$) and its 95% CI are calculated for Noah, and RMSEs ($m^3 m^{-3}$) between simulated and observed daily soil moisture are calculated for Srun, Vrun, and SVrun at seven states. The value that has a significant difference between tests and Noah control at the 95% CI is represented in boldface (decrease in italics).

Soil layer	Crun	Srun	Vrun	SVrun
AL				
5 cm	0.0685 ± 0.0012	0.0705 ± 0.0013	*0.0653* ± 0.0011	*0.0638* ± 0.0012
25 cm	0.0694 ± 0.0011	*0.0494* ± 0.0009	**0.0776** ± 0.0010	*0.0570* ± 0.0009
70 cm	0.1077 ± 0.0012	*0.0854* ± 0.0012	**0.1456** ± 0.0016	**0.1171** ± 0.0015
CO				
5 cm	0.0526 ± 0.0014	0.0534 ± 0.0014	0.0505 ± 0.0015	0.0508 ± 0.0015
25 cm	0.0616 ± 0.0013	**0.0644** ± 0.0013	**0.0696** ± 0.0014	**0.0719** ± 0.0015
MI				
5 cm	0.0540 ± 0.0019	0.0521 ± 0.0018	0.0554 ± 0.0019	0.0526 ± 0.0018
NE				
5 cm	0.0850 ± 0.0033	0.0848 ± 0.0012	0.0832 ± 0.0012	0.0896 ± 0.0013
25 cm	0.0463 ± 0.0017	*0.0301* ± 0.0006	*0.0231* ± 0.0008	*0.0231* ± 0.0009
70 cm	0.0270 ± 0.0008	0.0270 ± 0.0014	0.0270 ± 0.0014	0.0270 ± 0.0014
OK				
5 cm	0.0356 ± 0.0005	**0.0435** ± 0.0005	**0.0372** ± 0.0004	**0.0452** ± 0.0005
25 cm	0.0456 ± 0.0004	**0.0552** ± 0.0004	**0.0510** ± 0.0004	**0.0610** ± 0.0004
70 cm	0.0567 ± 0.0004	**0.0685** ± 0.0004	**0.0724** ± 0.0007	**0.0874** ± 0.0008
WTX				
5 cm	0.0360 ± 0.0008	*0.0343* ± 0.0007	0.0358 ± 0.0007	0.0360 ± 0.0007
25 cm	0.0791 ± 0.0023	*0.0743* ± 0.0023	0.0773 ± 0.0023	*0.0735* ± 0.0023
70 cm	0.0557 ± 0.0015	*0.0513* ± 0.0015	*0.0515* ± 0.0015	*0.0479* ± 0.0015
UT				
5 cm	0.0582 ± 0.0022	0.0562 ± 0.0022	*0.0536* ± 0.0021	*0.0532* ± 0.0021
25 cm	0.0599 ± 0.0019	0.0625 ± 0.0019	**0.0646** ± 0.0019	**0.0671** ± 0.0019

particularly for the shallow soil layer in AL and OK. This is most likely attributable to large differences in vegetation parameters (Figs. 3a,f). The increases in model accuracy (correlations and values of MAE and RMSE) are determined by the amount of disagreement between the NLDAS-2 and NASMD soil texture and vegetation types. The impact of these mismatches is also dependent on the soil layer and geographic location. The effects vary from month to month and, as expected, the impacts of vegetation mismatches are larger in summer than in winter.

2) IMPACTS ON EVAPOTRANSPIRATION

As shown in Fig. 2 and Eqs. (2)–(7), evapotranspiration is an important variable that affects soil moisture. At the same time, evapotranspiration is modulated by soil water content. Evapotranspiration generally increases as soil moisture and/or atmospheric demand increases. In regions where atmospheric demand for moisture exceeds soil moisture availability, evapotranspiration is constrained by soil moisture. Therefore, soil texture and vegetation differences not only affect soil moisture, but they also influence evapotranspiration. The comparisons between the daily evapotranspiration climatologies of Crun, Srun, Vrun, and SVrun are presented for AL, CO, MI, NE, OK, and WTX (Fig. 9). Not surprisingly, changes in only the soil texture parameter do not result in large changes in evapotranspiration. However, the differences between SVrun and Crun or Vrun and Crun are large, suggesting that vegetation mismatches have a much larger impact on variations in the evapotranspiration climatology than soil texture mismatches. This makes sense because vegetation type directly controls evapotranspiration through rooting depth and canopy resistance and indirectly controls evapotranspiration through soil moisture, as discussed in section 3a. Overall, the site-specific vegetation from NASMD generates lower evapotranspiration compared to the default Noah vegetation for all regions and seasons, except for spring and early summer in AL, MI, and OK. These results suggest that mismatches in vegetation type that lead to an underestimation (overestimation) of ET result in overly wet (dry) soils in the root zone. However, results suggested that mismatched vegetation type most often leads to overestimation of ET in Crun compared to Vrun and SVrun. These errors in ET estimation can provide feedback to boundary layer processes that will result in enhanced or diminished moisture flux.

b. Pointwise analysis from soil and vegetation change experiments

As discussed in section 4a, soil texture and vegetation type mismatches have significant impacts on soil moisture variations (correlation) and magnitude (MAE and

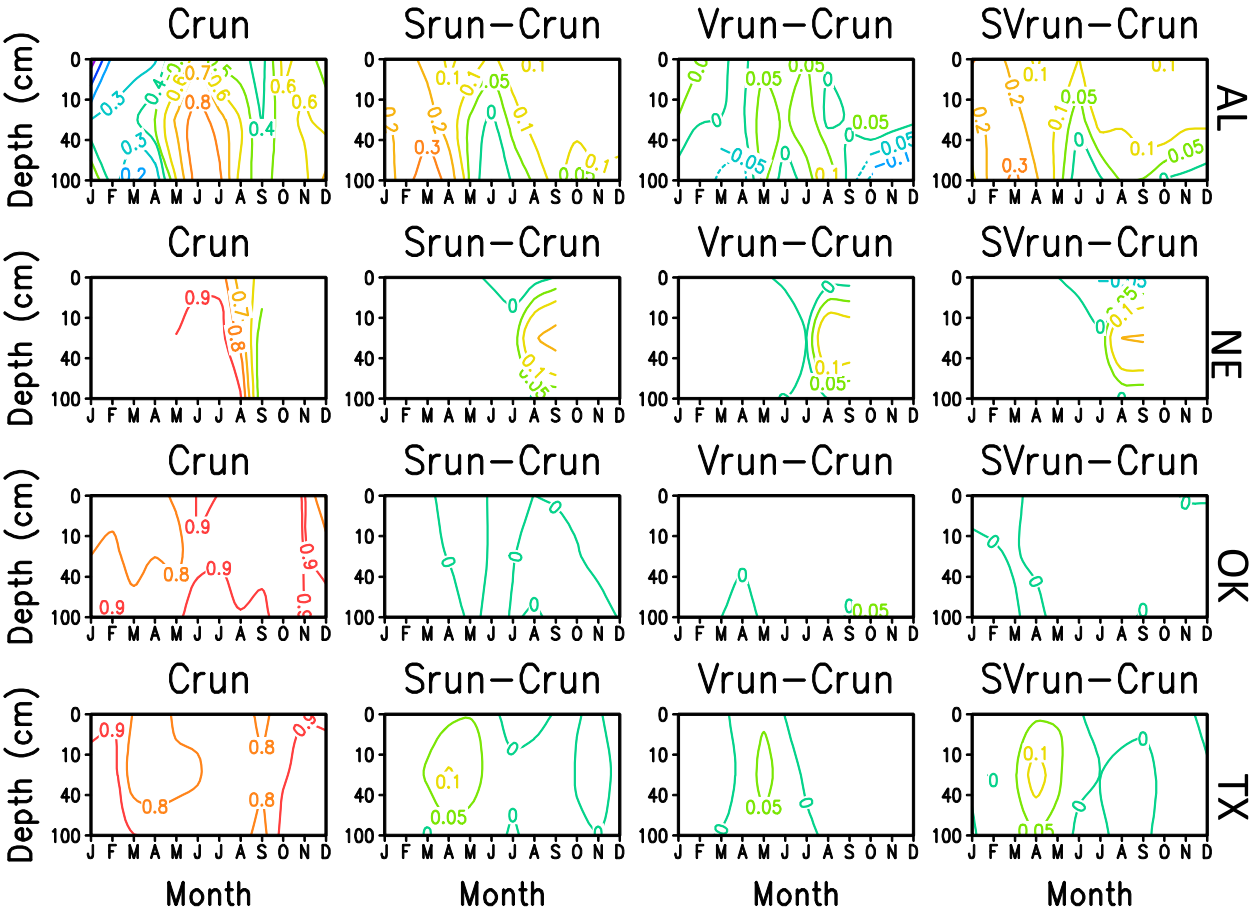

FIG. 5. Variation of anomaly correlation between simulated and observed daily soil moisture and their differences (Srun − Crun, Vrun − Crun, and SVrun − Crun) with soil depth and month in AL, NE, OK, and WTX (TX). Differences outside of ±0.05 are significant at the 95% confidence level. Positive differences denote improvement/increase in anomaly correlation.

RMSE). Greater evapotranspiration in spring and summer in Crun results in decreased summertime deep-layer soil moisture as compared to Vrun. This results in larger MAE values in the summer. Because of the effect of multiple sites being averaged for each region, it is not clear if Crun reasonably represents the impact of changes in soil texture and vegetation type on evapotranspiration, total runoff, and soil moisture. These impacts are subsequently analyzed at two selected grid points: MI1 (41.81°N, 83.81°W) and TX1 (33.19°N, 101.34°W). These two sites were selected because they have the same vegetation type and large mismatches in soil texture. The results show that sites with loam (clay) soils have more (less) evapotranspiration, lower (higher) soil moisture content, and less (more) total runoff. This manifests as differences in evapotranspiration, soil moisture, and runoff between Crun and Srun at the MI1 and TX1 sites. The results suggest that Noah can reasonably simulate the qualitative impact of soil texture change on evapotranspiration, runoff, and soil moisture, although this impact may be small on evapotranspiration and total runoff (Fig. 10).

A comparison of simulated evapotranspiration, total runoff, and soil moisture for Crun and Vrun is performed (Fig. 11) at two selected grid points, AL1 (34.19°N, 87.19°W) and CO1 (39.69°N, 105.69°W). These two sites are selected because they have the same soil texture (i.e., sandy loam) and large mismatches in vegetation type. Site CO1 is a mountain location with substantial

TABLE 4. The variation of daily anomaly correlation (all values are significant at the 95% confidence level) with month and depth in CO, MI, and UT for the warm season for Crun.

Month	CO at 5 cm	CO at 25 cm	MI at 5 cm	UT at 5 cm	UT at 25 cm
May	0.59	0.67	0.63	0.51	0.50
Jun	0.59	0.83	0.60	0.74	0.91
Jul	0.57	0.64	0.70	0.61	0.90
Aug	0.71	0.81	0.74	0.71	0.68
Sep	0.70	0.58	0.72	0.77	0.70

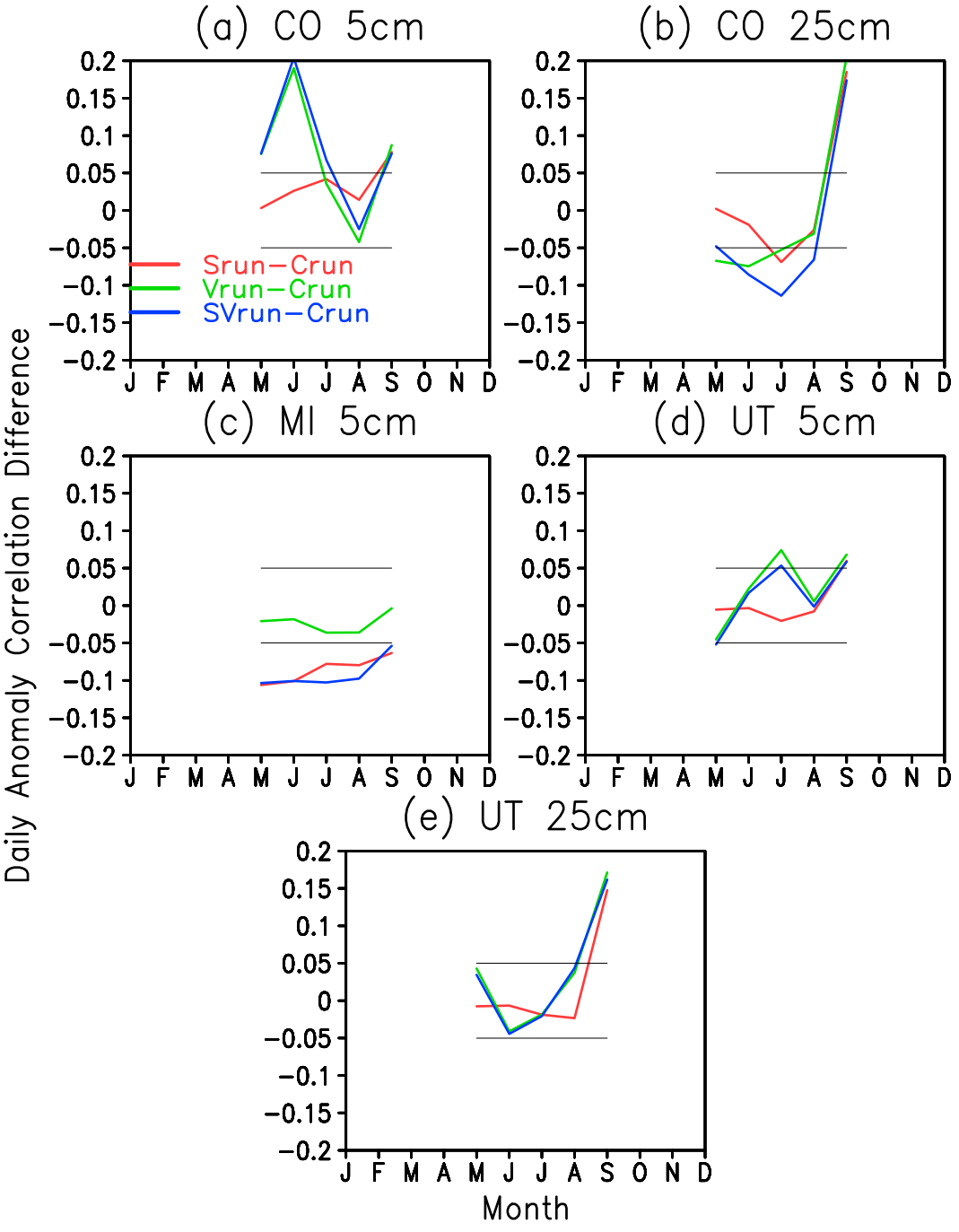

FIG. 6. Difference of anomaly correlation between simulated and observed daily soil moisture [Srun − Crun (red line), Vrun − Crun (green line), and SVrun − Crun (blue line)] from month to month in (a) CO at 5 cm, (b) CO at 25 cm, (c) MI at 5 cm, (d) UT at 5 cm, and (e) UT at 25 cm. Differences outside of ±0.05 are significant at the 95% confidence level. Positive differences denote improvement/increase in anomaly correlation.

snowmelt in spring. This has a large impact on the seasonal cycle of total runoff (Fig. 11b) and soil moisture (Figs. 11c–f). The vegetation type at AL1 is evergreen needleleaf forest for Crun and grass for Vrun. At CO1, Crun is set to grass and Vrun is set to mixed forest. The results show that forest and mixed forest generate larger evapotranspiration, less total runoff, and less soil moisture than grass, as expected. However, the differences in soil moisture in the 1–2-m soil layer (i.e., SM4) are smaller than in other layers, despite large differences in

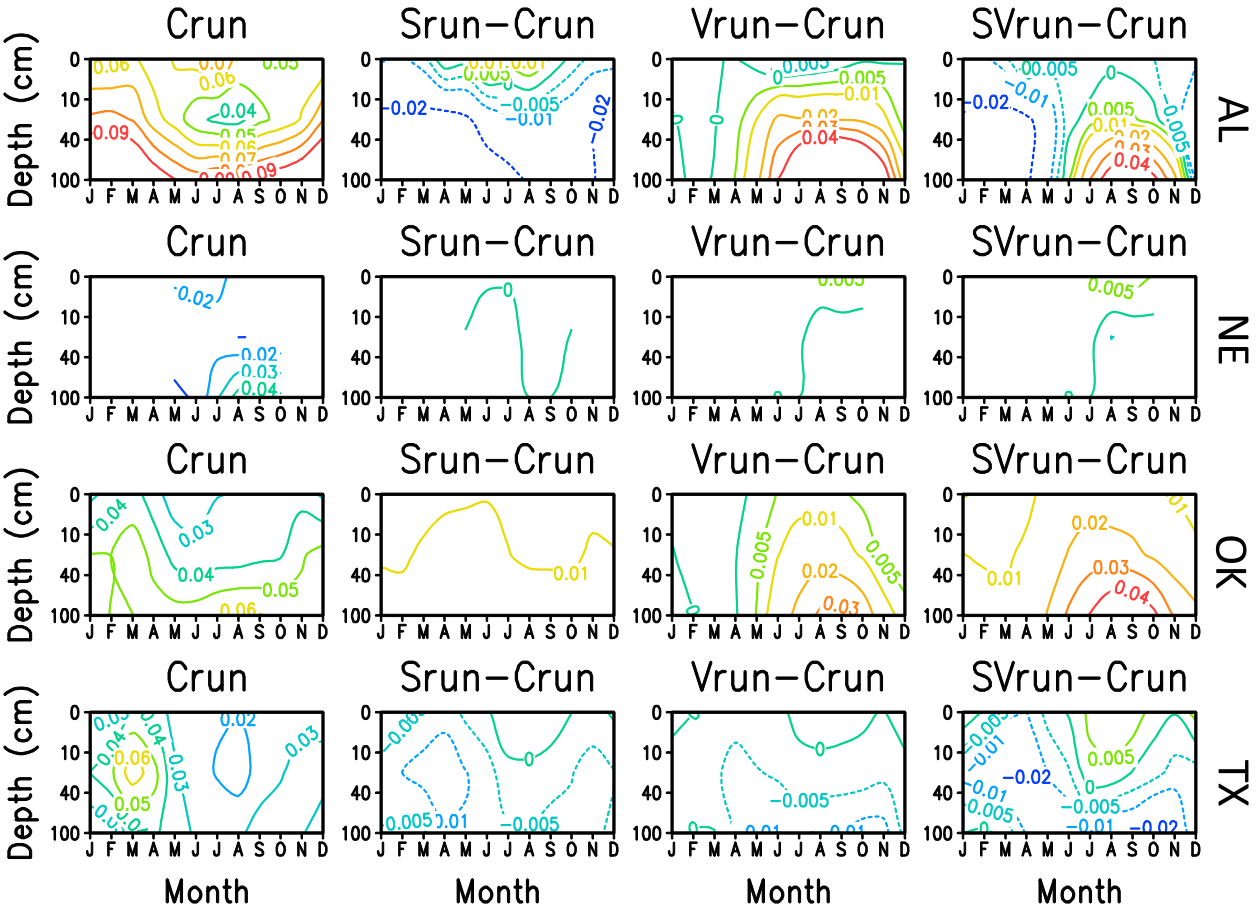

FIG. 7. Variation of MAE ($m^3\,m^{-3}$) between simulated and observed daily soil moisture and their differences (Srun − Crun, Vrun − Crun, and SVrun − Crun) with soil depth and month in AL, NE, OK, and WTX (TX). Differences outside of ±0.01 are significant at the 95% confidence level. Negative differences denote improvement/reduction increase in MAE.

rooting depth between the vegetation types. The reasons for this phenomenon are unclear and need further investigation. It is possible that the 10-yr spinup is not sufficient for Vrun when there are large vegetation mismatches (e.g., from grass to forest or from forest to grass). At CO1, there is a shift in the timing of peak runoff and soil moisture in the first three soil layers when vegetation type is changed from grass to mixed cover. This is because changes in vegetation lead to changes in the timing of snowmelt. In particular for this experiment, it looks like forest leads to earlier and faster snowmelt. Overall, these results indicate that Noah can reasonably simulate the qualitative impact that changes in vegetation type have on evaporation, total runoff, and soil moisture. The quantitative impact is difficult to assess and examine in this study and needs further investigation. These results further highlight the importance of improving the representativeness of soil texture and vegetation type. This can be accomplished through adding high-resolution model configurations, such as the tiling approach that is currently under development and that will be included in future versions of Noah.

5. Conclusions

Soil moisture simulations include many complex linear and nonlinear physical processes. Simulation errors can arise from 1) errors in the forcing data; 2) errors in the model structure, as described in the first part of our companion paper (Xia et al. 2015); and/or 3) errors in model parameters such as soil texture and vegetation type mismatches. This paper investigates the impact of soil texture and vegetation type mismatches on soil moisture, evapotranspiration, and total runoff. The results show that Noah is sensitive to changes in soil texture and vegetation type in most regions and soil layers, and the sensitivity varies depending on the time of the year. The results presented here are mixed; the use of site-observed soil texture and vegetation type does not necessarily improve soil moisture simulations (i.e., it

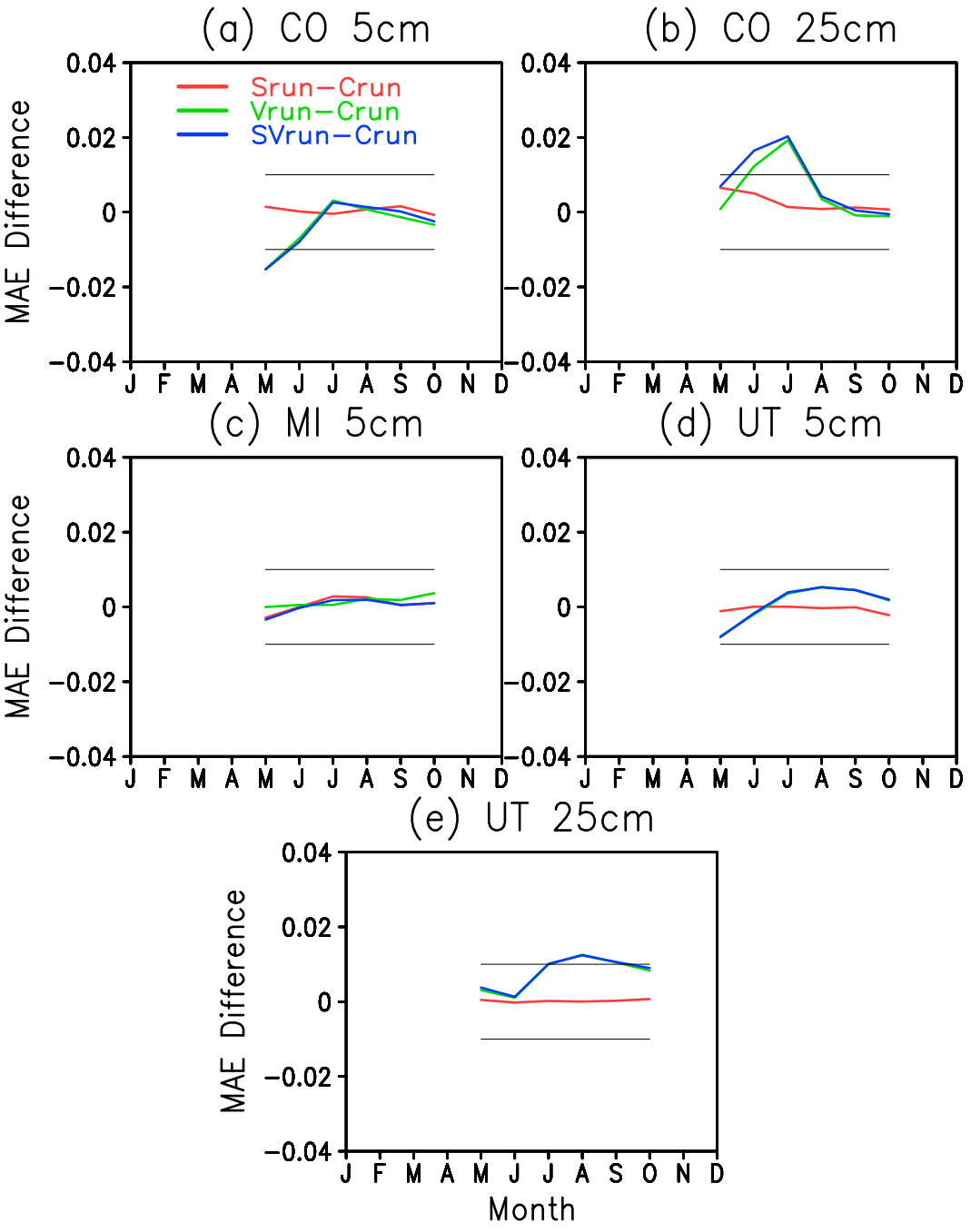

FIG. 8. Difference of MAE ($m^3\ m^{-3}$) between simulated and observed daily soil moisture [Srun − Crun (red line), Vrun − Crun (green line), and SVrun − Crun (blue line)] from month to month in (a) CO at 5 cm, (b) CO at 25 cm, (c) MI at 5 cm, (d) UT at 5 cm, and (e) UT at 25 cm. Differences outside of ±0.01 are significant at the 95% confidence level. Negative differences denote improvement/reduction increase in MAE.

does not increase anomaly correlation and decrease MAE and RMSE values for all regions and soil layers). Noah is relatively well calibrated with the model-specified soil textures and vegetation types (Livneh et al. 2010; Smith et al. 2012; Wei et al. 2013) so that compensation effects (e.g., effect of the ill-calibrated model parameters from model-specified soil texture and vegetation type) may exist in Noah. The pointwise analysis shows that Noah can reasonably simulate variations in daily evapotranspiration, soil moisture, and total runoff when soil texture (vegetation type) is changed from loam (forest) to clay (grasslands), or vice versa. This suggests that the

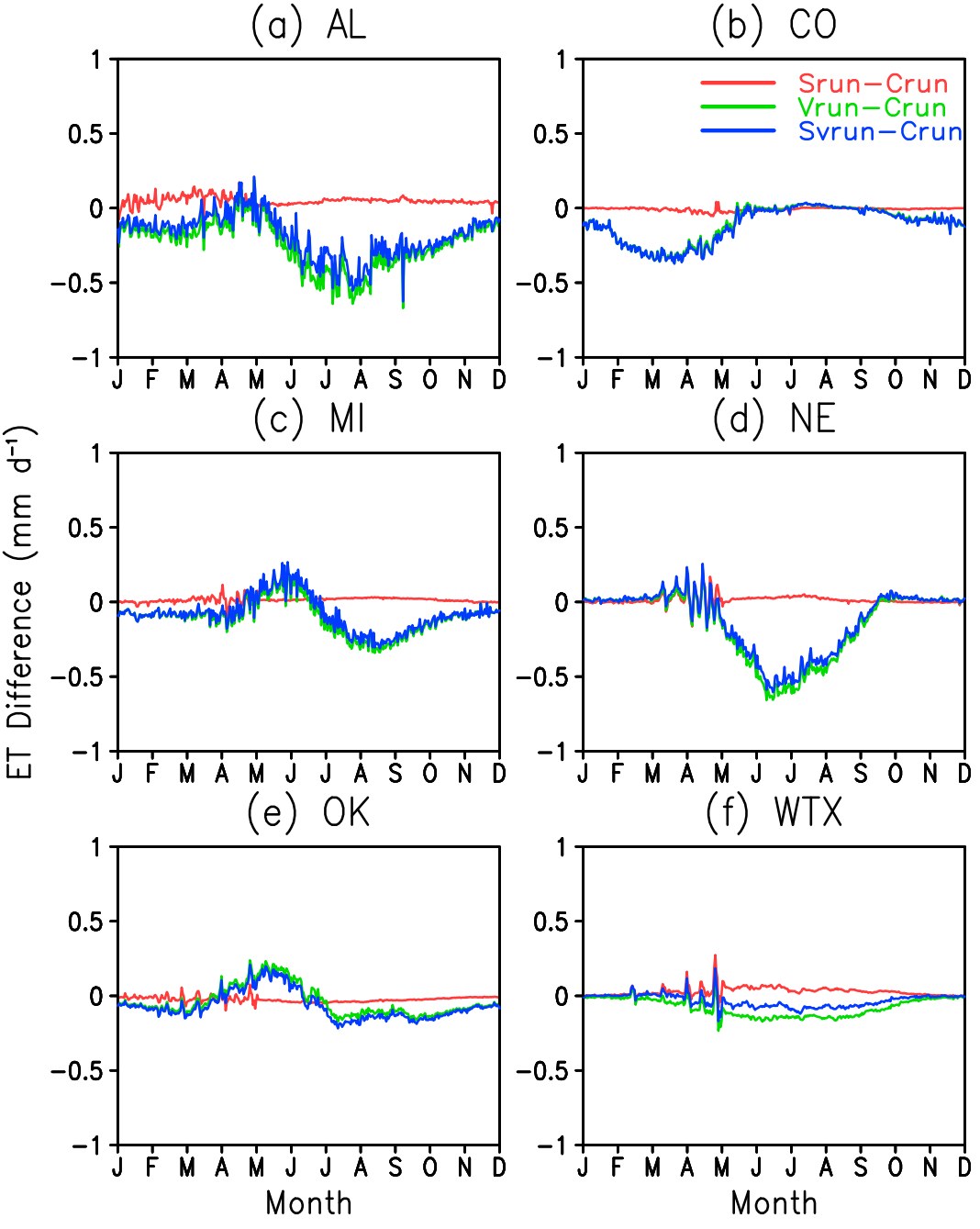

FIG. 9. Differences of simulated daily evapotranspiration climatology [Srun − Crun (red line), Vrun − Crun (green line), and SVrun − Crun (blue line)] in (a) AL, (b) CO, (c) MI, (d) NE, (e) OK, and (f) WTX.

performance of Noah can be further improved by tuning model parameters using site-observed soil texture and vegetation type as was done in Wei et al. (2013). It should be noted that this study was performed using only Noah. Similar studies using the other three NLDAS-2 models will be addressed in a future paper.

All of the sensitivity tests undertaken in this study strictly follow the NLDAS-2 configuration and experimental design without any extra calibration. It is recognized that this is a fairly simplistic study (e.g., parameter swapping) with many limitations. Some more robust methods such as using a Monte Carlo sampling procedure (Spear and Hornberger 1980; Wagener et al. 2001), generalized likelihood uncertainty estimation (GLUE; Beven and Binley 1992; Beven 2002), Bayesian stochastic inversion (BSI; Jackson et al. 2003; Xia et al. 2004), and

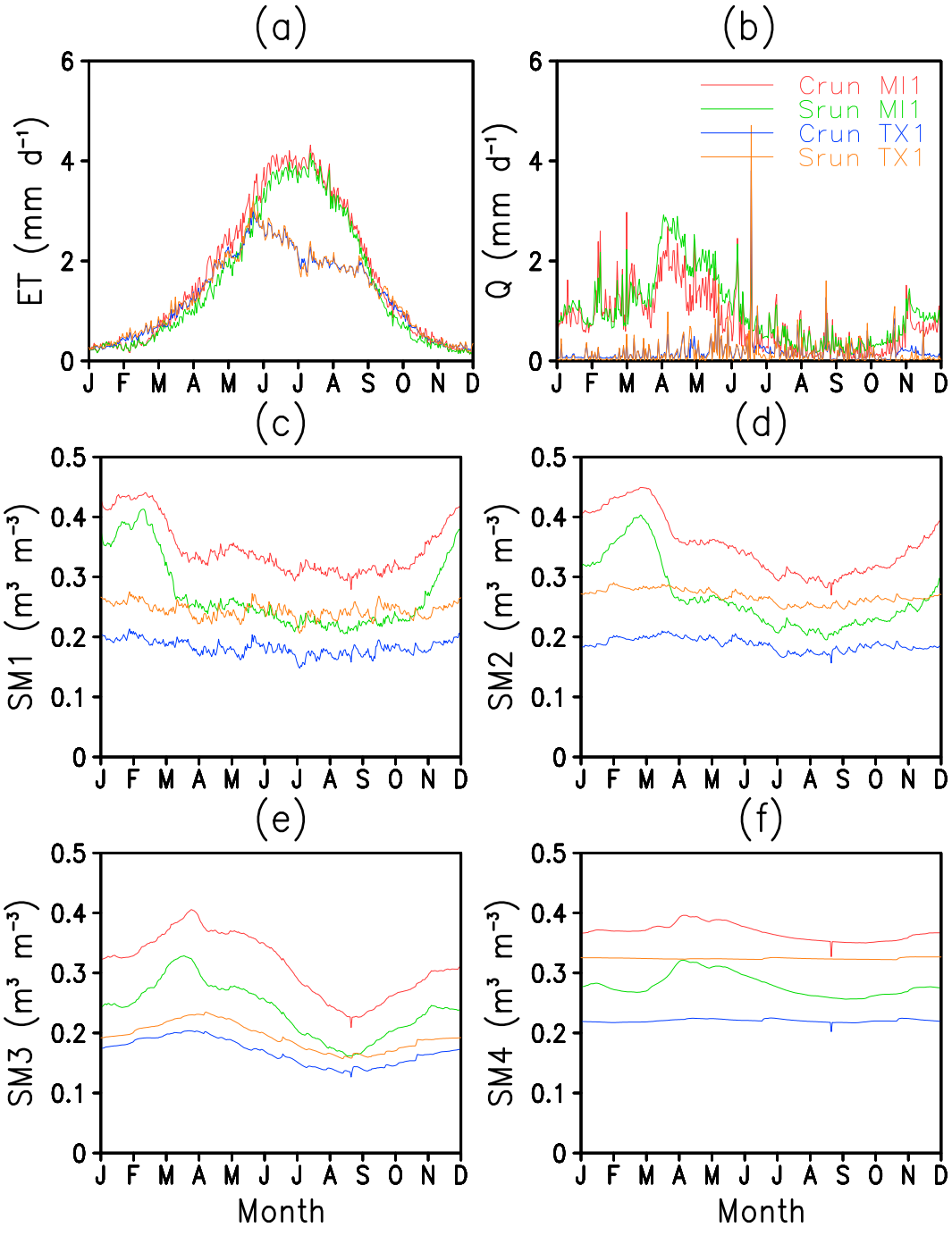

FIG. 10. Comparison of simulated (a) evapotranspiration, (b) total runoff, (c) 5-cm soil moisture (SM1), (d) 25-cm soil moisture (SM2), (e) 70-cm soil moisture (SM3), and (f) 150-cm soil moisture (SM4) at two points: MI1 (41.81°N, 83.81°W) in Michigan and TX1 (33.19°N, 101.34°W) in West Texas. At MI1, soil texture is changed from loam (red line) into clay (green line). At TX1, soil texture is changed from clay (blue line) into loam (orange line).

the complex approach used in Rosero et al. (2009, 2010) are more appropriate for performing parameter sensitivity tests to investigate the impacts of model parameters on water fluxes, energy fluxes, and the simulation of state variables. These approaches will be applied in the future studies using the other three NLDAS-2 models.

Noah has simple soil hydrology, soil physics, and vegetation dynamics, with the soil texture in the top 5 cm

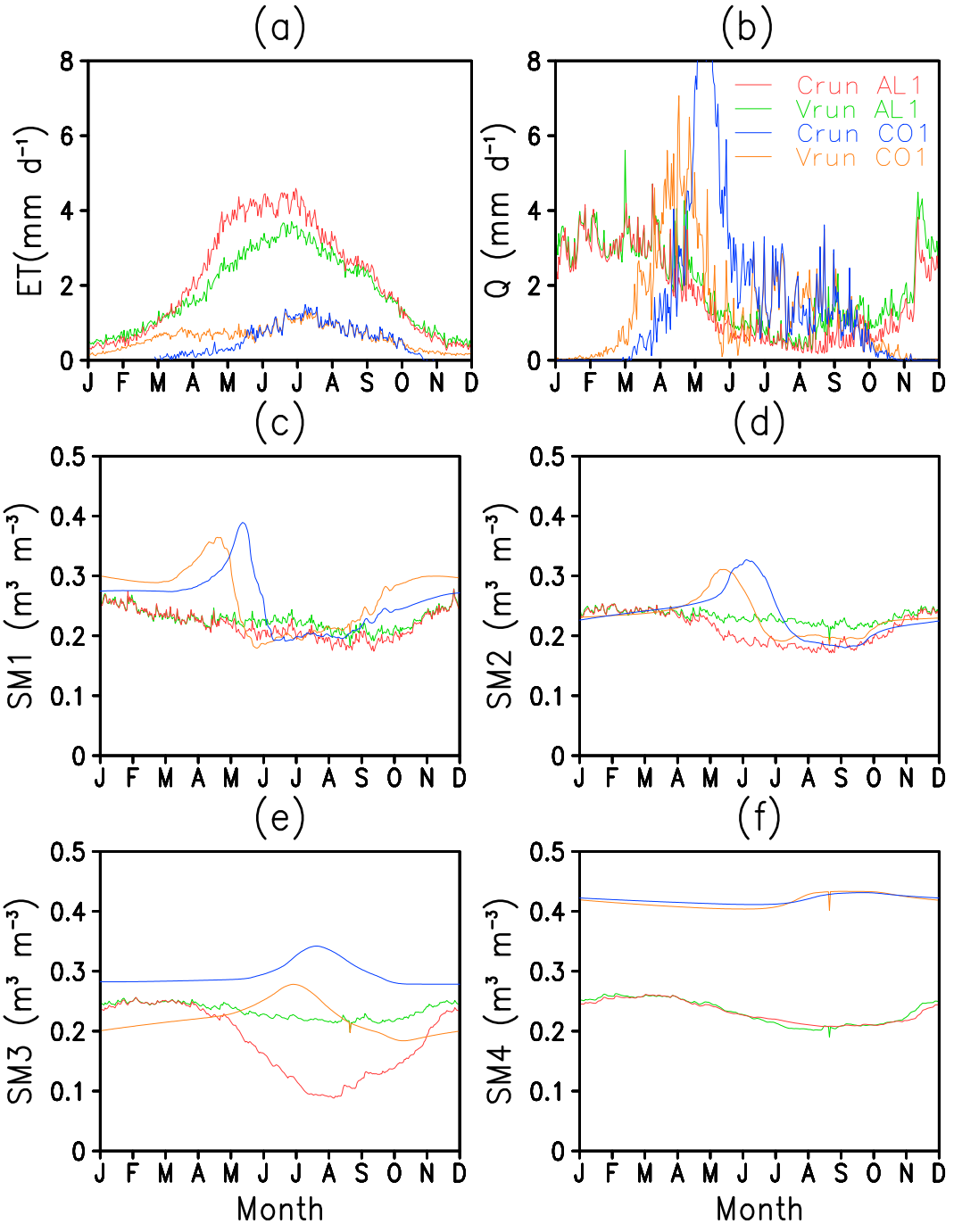

FIG. 11. As in Fig. 10, but for AL1 (34.19°N, 87.19°W) in Alabama and CO1 (39.69°N, 105.69°W) in Colorado. At AL1, vegetation type is changed from deciduous needleleaf forest (red line) into grasslands (green line). At CO1, vegetation type is changed from grasslands (blue line) into mixed cover (orange line).

representing the soil texture in the entire 2-m soil column (four soil layers) for a given 1/8° grid cell. In the real world, soil texture is not homogeneous with depth (or over space). This heterogeneity will lead to the variations in the corresponding soil and hydraulic parameters (Peschel et al. 2006). Noah also uses a single dominant vegetation type for each grid cell. Noah does not consider any subgrid tiling of soil and vegetation parameters. These issues may be overcome by adding spatial tiling or subgrid process for soil and vegetation classification and adding more reasonable soil profiles with depth-varying soil textures. In addition, it is recommended that the

equations from Cosby et al. (1984) be used to recalculate the parameters in each soil layer in Noah when the percentages of sand, silt, and clay are known. This will help to avoid the soil texture classification issues identified in this study. These issues will be addressed in the future by the NCEP/EMC Noah development team and its collaborators.

Acknowledgments. The authors thank Prof. Ken Hubbard from University of Nebraska–Lincoln and Dr. Jeff Andersen from Michigan State University, who gave us measurement error estimates and suggested that we not use measured soil moisture during the cold season. Y.X. was sponsored by the NOAA Climate Program Office's Modeling, Analyses, Predictions, and Projections (MAPP) Program. S.Q. and T.F. were funded by the National Science Foundation (Award AGS-1056796). Y.X. also thanks Jesse Meng and Helin Wei for the helpful discussions and Jongil Han and Yan Luo from EMC for the beneficial comments. We thank all three reviewers for their comments and edits. They greatly improved the quality and readability of this manuscript.

REFERENCES

Beven, K. J., 2002: Towards a coherent philosophy for modelling the environment. *Proc. Roy. Soc. London*, **458**, 2465–2484, doi:10.1098/rspa.2002.0986.

——, and A. M. Binley, 1992: The future of distributed models: Model calibration and uncertainty prediction. *Hydrol. Processes*, **6**, 279–298, doi:10.1002/hyp.3360060305.

Chen, F., and J. Dudhia, 2001: Coupling an advanced land surface–hydrology model with the Penn State–NCAR MM5 modeling system. Part I: Model implementation and sensitivity. *Mon. Wea. Rev.*, **129**, 569–585, doi:10.1175/1520-0493(2001)129<0569:CAALSH>2.0.CO;2.

——, and Coauthors, 1996: Modeling of land surface evaporation by four schemes and comparison with FIFE observations. *J. Geophys. Res.*, **101**, 7251–7268, doi:10.1029/95JD02165.

Congalton, R. G., and K. Green, 2009: *Assessing the Accuracy of Remotely Sensed Data: Principles and Practices.* CRC Press, 179 pp.

Cosby, B., G. M. Hornberger, R. B. Clapp, and T. R. Ginn, 1984: A statistical exploration of the relationships of soil moisture characteristics to the physical properties of soils. *Water Resour. Res.*, **20**, 682–690, doi:10.1029/WR020i006p00682.

Cosgrove, B. A., and Coauthors, 2003: Land surface model spin-up behavior in the North American Land Data Assimilation System (NLDAS). *J. Geophys. Res.*, **108**, 8845, doi:10.1029/2002JD003316.

Dickinson, R. E., A. Henderson-Sellers, and P. J. Kennedy, 1993: Biosphere–Atmosphere Transfer Scheme (BATS) Version 1e as coupled to the NCAR Community Climate Model. NCAR Tech. Note NCAR-TN-387+STR, 88 pp., doi:10.5065/D67W6959.

Ek, M. B., 2005: *Interactions of the Land-Surface with the Atmospheric Boundary Layer.* Ponesen & Looijen, 210 pp.

——, and L. Mahrt, 1991: OSU 1-D PBL model user's guide. Dept. of Atmospheric Sciences, Oregon State University, Corvallis, OR, 117 pp.

——, and A. A. M. Holtslag, 2004: Influence of soil moisture on boundary layer cloud development. *J. Hydrometeor.*, **5**, 86–99, doi:10.1175/1525-7541(2004)005<0086:IOSMOB>2.0.CO;2.

——, K. E. Mitchell, Y. Lin, E. Rodgers, P. Grunman, V. Koren, G. Gayno, and J. D. Tarpley, 2003: Implementation of Noah land surface model advances in the National Centers for Environmental Prediction operational mesoscale Eta model. *J. Geophys. Res.*, **108**, 8851, doi:10.1029/2002JD003296.

Fernandez-Illescas, C. P., A. Porporato, F. Laio, and I. Rodriguez-Iturbe, 2001: The ecohydrological role of soil texture in a water-limited ecosystem. *Water Resour. Res.*, **37**, 2863–2872, doi:10.1029/2000WR000121.

Hansen, M. C., R. S. DeFries, J. R. G. Townshend, and R. Sohlberg, 2000: Global land cover classification at 1 km spatial resolution using a classification tree approach. *Int. J. Remote Sens.*, **21**, 1331–1364, doi:10.1080/014311600210209.

Hodnett, M. G., L. Pimentel da Silva, H. R. da Rocha, and R. Cruz Senna, 1995: Seasonal soil water storage changes beneath central Amazonian rainforest and pasture. *J. Hydrol.*, **170**, 233–254, doi:10.1016/0022-1694(94)02672-X.

Hotelling, H., 1953: New light on the correlation coefficient and its transforms. *J. Roy. Stat. Soc.*, **15B**, 193–225.

Illston, B. G., J. B. Basara, D. K. Fischer, R. L. Elliott, C. Fiebrich, K. C. Crawford, K. Humes, and E. Hunt, 2008: Mesoscale monitoring of soil moisture across a statewide network. *J. Atmos. Oceanic Tech.*, **25**, 167–182, doi:10.1175/2007JTECHA993.1.

Jackson, C., Y. Xia, M. Sen, and P. Stoffa, 2003: Optimal parameter and uncertainty estimation of a land surface model: A case example using data from Cabauw, Netherlands. *J. Geophys. Res.*, **108**, 4583, doi:10.1029/2002JD002991.

Jacquemin, B., and J. Noilhan, 1990: Sensitivity study and validation of a land surface parameterization using the HAPEX-MOBILHY data set. *Bound.-Layer Meteor.*, **52**, 93–134, doi:10.1007/BF00123180.

Jarvis, P. G., 1976: The interaction of the variation in leaf water potential and stomatal conductance found in canopies in the field. *Philos. Trans. Roy. Soc. London*, **B273**, 593–610, doi:10.1098/rstb.1976.0035.

Koster, R., and M. Suarez, 1996: Energy and water balance calculations in the Mosaic LSM. NASA Tech. Memo. 104606, Vol. 9, 60 pp. [Available online at http://gmao.gsfc.nasa.gov/pubs/docs/Koster130.pdf.]

Kumar, S. V., R. Reichle, R. Koster, W. Crow, and C. Peters-Lidard, 2009: Role of subsurface physics in the assimilation of surface soil moisture observations. *J. Hydrometeor.*, **10**, 1534–1547, doi:10.1175/2009JHM1134.1.

——, and Coauthors, 2014: Assimilation of remotely sensed soil moisture and snow depth retrievals for drought estimation. *J. Hydrometeor.*, **15**, 2446–2469, doi:10.1175/JHM-D-13-0132.1.

Livneh, B., Y. Xia, K. E. Mitchell, M. B. Ek, and D. P. Lettenmaier, 2010: Noah LSM snow model diagnostics and enhancements. *J. Hydrometeor.*, **11**, 721–738, doi:10.1175/2009JHM1174.1.

Mahrt, L., and M. Ek, 1984: The influence of atmospheric stability on potential evaporation. *J. Climate Appl. Meteor.*, **23**, 222–234, doi:10.1175/1520-0450(1984)023<0222:TIOASO>2.0.CO;2.

McNaughton, K. G., and P. G. Jarvis, 1983: Predicting the effects of vegetation changes on transpiration and evaporation. *Additional Woody Crop Plants*, T. T. Kozlowski, Ed., Vol. VII, *Water Deficits and Plant Growth*, Academic, 1–47, doi:10.1016/B978-0-12-424157-2.50007-0.

Miller, D. A., and R. A. White, 1998: A conterminous United States multilayer soil characteristics dataset for regional

climate and hydrology modeling. *Earth Interact.*, **2**, doi:10.1175/1087-3562(1998)002<0001:ACUSMS>2.3.CO;2.

Nepstad, D. C., and Coauthors, 1994: The role of deep roots in the hydrological and carbon cycles of Amazonian forest and pasture. *Nature*, **372**, 666–669, doi:10.1038/372666a0.

Noilhan, J., and S. Planton, 1989: A simple parameterization of land surface processes for meteorological models. *Mon. Wea. Rev.*, **117**, 536–549, doi:10.1175/1520-0493(1989)117<0536:ASPOLS>2.0.CO;2.

Peschel, J. M., P. K. Haan, and R. E. Lacey, 2006: Influences of soil data set resolution on hydrologic modeling. *J. Amer. Water Resour. Assoc.*, **42**, 1371–1389, doi:10.1111/j.1752-1688.2006.tb05619.x.

Rawls, W. J., T. J. Gish, and D. L. Brakensiek, 1991: Estimating soil water retention from soil physical properties and characteristics. *Advances in Soil Science*, Vol. 16, B. A. Stewart, Ed., Springer, 213–234.

Reichle, R. H., R. D. Koster, J. Dong, and A. A. Berg, 2004: Global soil moisture from satellite observations, land surface models, and ground data: Implications for data assimilation. *J. Hydrometeor.*, **5**, 430–442, doi:10.1175/1525-7541(2004)005<0430:GSMFSO>2.0.CO;2.

Reynolds, C. A., T. J. Jackson, and W. J. Rawls, 2000: Estimating soil water-holding capacities by linking the Food and Agriculture Organization soil map of the world with global pedon databases and continuous pedotransfer functions. *Water Resour. Res.*, **36**, 3653–3662, doi:10.1029/2000WR900130.

Rosero, E., Z. L. Yang, L. E. Gulden, G. Y. Niu, and D. J. Gochis, 2009: Evaluating enhanced hydrological representations in Noah LSM over transition zones: Implications for model development. *J. Hydrometeor.*, **10**, 600–622, doi:10.1175/2009JHM1029.1.

——, ——, T. Wagener, L. E. Gulden, S. Yatheendradas, and G. Y. Niu, 2010: Quantifying parameter sensitivity, interaction, and transferability in hydrologically enhanced versions of the Noah land surface model over transition zones during the warm season. *J. Geophys. Res.*, **115**, D03106, doi:10.1029/2009JD012035.

Santanello, J. A., S. V. Kumar, C. D. Peters-Lidard, K. Harrison, and S. Zhou, 2013: Impact of land model calibration on coupled land–atmosphere prediction. *J. Hydrometeor.*, **14**, 1373–1400, doi:10.1175/JHM-D-12-0127.1.

Saville, D. J., 1990: Multiple comparison procedures: The practical solution. *Amer. Stat.*, **44**, 174–180, doi:10.1080/00031305.1990.10475712.

Schaake, J. C., V. I. Koren, Q. Y. Duan, K. Mitchell, and F. Chen, 1996: Simple water balance model for estimating runoff at different temporal and spatial scales. *J. Geophys. Res.*, **101**, 7461–7475, doi:10.1029/95JD02892.

Schroeder, J. L., W. S. Burgett, K. B. Haynie, I. Sonmez, G. D. Skwira, A. L. Doggett, and J. W. Lipe, 2005: The West Texas Mesonet: A technical overview. *J. Atmos. Oceanic Technol.*, **22**, 211–222, doi:10.1175/JTECH-1690.1.

Smith, M. B., and Coauthors, 2012: Results of DMIP2 Oklahoma experiments. *J. Hydrol.*, **418–419**, 17–48, doi:10.1016/j.jhydrol.2011.08.056.

Spear, R. C., and G. M. Hornberger, 1980: Eutrophication in Peel inlet—II. Identification of critical uncertainties via generalized sensitivity analysis. *Water Res.*, **14**, 43–49, doi:10.1016/0043-1354(80)90040-8.

Steiger, J. H., 1980: Tests for comparing elements of a correlation matrix. *Psychol. Bull.*, **87**, 245–251, doi:10.1037/0033-2909.87.2.245.

Swank, W., and J. Douglass, 1974: Streamflow greatly reduced by converting deciduous hardwood stands to pine. *Science*, **185**, 857–859, doi:10.1126/science.185.4154.857.

Tennant, D., 1976: Wheat crop penetration and total available water on a range of soil types. *Aust. J. Exp. Agric. Anim. Husb.*, **16**, 570–577, doi:10.1071/EA9760570.

Turner, K. M., 1991: Annual evapotranspiration of native vegetation in a Mediterranean-type climate. *J. Amer. Water Resour. Assoc.*, **27**, 1–6, doi:10.1111/j.1752-1688.1991.tb03107.x.

Wagener, T., D. P. Boyle, M. J. Lees, H. S. Wheater, H. V. Gupta, and S. Sorooshian, 2001: A framework for development and application of hydrological models. *Hydrol. Earth Syst. Sci.*, **5**, 13–26, doi:10.5194/hess-5-13-2001.

Wang, T., E. Istanbulluoglu, J. Lenters, and D. Scott, 2009: On the role of groundwater and soil texture in the regional water balance: An investigation of the Nebraska Sand Hills, USA. *Water Resour. Res.*, **45**, W10413, doi:10.1029/2009WR007733.

Wei, H., Y. Xia, K. E. Mitchell, and M. B. Ek, 2013: Improvement of the Noah land surface model for warm season processes: evaluation of water and energy flux simulation. *Hydrol. Processes*, **27**, 297–303, doi:10.1002/hyp.9214.

Xia, Y., M. K. Sen, C. S. Jackson, and P. L. Stoffa, 2004: Multidataset study of optimal parameter and uncertainty estimation of a land surface model with Bayesian stochastic inversion and multicriteria method. *J. Appl. Meteor.*, **43**, 1477–1497, doi:10.1175/JAM2145.1.

——, and Coauthors, 2012a: Continental-scale water and energy flux analysis and validation for the North American Land Data Assimilation System project phase 2 (NLDAS-2): 1. Intercomparison and application of model products. *J. Geophys. Res.*, **117**, D03109, doi:10.1029/2011JD016048.

——, and Coauthors, 2012b: Continental-scale water and energy flux analysis and validation for North American Land Data Assimilation System project phase 2 (NLDAS-2): 2. Validation of model-simulated streamflow. *J. Geophys. Res.*, **117**, D03110, doi:10.1002/2013JD020994.

——, J. Sheffield, M. B. Ek, J. Dong, N. Chaney, H. Wei, J. Meng, and E. F. Wood, 2014: Evaluation of multi-model simulated soil moisture in NLDAS-2. *J. Hydrol.*, **512**, 107–125, doi:10.1016/j.jhydrol.2014.02.027.

——, M. B. Ek, Y. Wu, T. W. Ford, and S. M. Quiring, 2015: Comparison of NLDAS-2 simulated and NASMD observed daily soil moisture. Part I: Comparison and analysis. *J. Hydrometeor.*, **16**, 1962–1980, doi:10.1175/JHM-D-14-0096.1.

Zhang, L., W. R. Dawes, and G. R. Walker, 2001: Response of mean annual evapotranspiration to vegetation change at catchment scale. *Water Resour. Res.*, **37**, 701–708, doi:10.1029/2000WR900325.